Bioelectrochemistry

International Edition: DOI: 10.1002/anie.201504188
German Edition: DOI: 10.1002/ange.201504188

Reversible Switching of Redox-Active Molecular Orbitals and Electron Transfer Pathways in Cu_A Sites of Cytochrome *c* Oxidase**

*Ulises Zitare, Damián Alvarez-Paggi, Marcos N. Morgada, Luciano A. Abriata, Alejandro J. Vila, and Daniel H. Murgida**

Abstract: *The Cu_A site of cytochrome c oxidase is a redox hub that participates in rapid electron transfer at low driving forces with two redox cofactors in nearly perpendicular orientations. Spectroscopic and electrochemical characterizations performed on first and second-sphere mutants have allowed us to experimentally detect the reversible switching between two alternative electronic states that confer different directionalities to the redox reaction. Specifically, the M160H variant of a native Cu_A shows a reversible pH transition that allows to functionally probe both states in the same protein species. Alternation between states exerts a dramatic impact on the kinetic redox parameters, thereby suggesting this effect as the mechanism underlying the efficiency and directionality of Cu_A electron transfer in vivo. These findings may also prove useful for the development of molecular electronics.*

Protein electron-transfer (ET) reactions constitute the basis of energy transduction in living organisms and involve a plethora of fine-tuning mechanisms that have just begun to be uncovered. This variety arises from the structural complexity of redox proteins,[1] and includes modulation of the electronic coupling (H_{DA}) by fluctuations of the amino acidic bridge between donor and acceptor[2–5] and tuning of reorganization energies (λ) by second-sphere ligands,[6] among other possibilities.

The Cu_A site is the primary electron acceptor of the terminal respiratory enzyme cytochrome c oxidase (CcO), which acts as a proton pump while sequentially transferring electrons through several redox cofactors towards molecular oxygen.[7] The two Cu ions of the binuclear center are bridged by cysteine ligands, forming a nearly planar Cu_2S_2 diamond core characterized by a short Cu–Cu distance. The coordination sphere is completed by two equatorial histidines and two weak axial ligands provided by a methionine (M160) sulfur and a backbone carbonyl group.[8]

The electronic structure of Cu_A can be described by a double-well potential as a function of small geometric perturbations, such as Cu–Cu stretching[9] or dihedral distortions,[10] where the energy minima correspond to two alternative σ_u^* and π_u ground states (GSs). As determined for the Cu_A-containing subunit II fragment of the ba_3 oxidase from *Thermus thermophilus* (*Tt*-Cu_A), the π_u state is thermally accessible at room temperature from the lower lying σ_u^* state.[11] Moreover, NMR and DFT calculations show differential electron densities in the σ_u^* and π_u GSs, thus leading to the proposal that both states may be functional in vivo, conferring directionality by means of differential electronic coupling of Cu_A in the different GSs with the electron donor (cytochrome *c*) and acceptor (a heme cofactor), respectively.[10] In recent work we reported that the σ_u^*/π_u energy gap ($\Delta E_{\sigma_u^*/\pi_u}$) can be fine-tuned either by mutating the weak axial ligand M160 or by substituting the three loops that define the second coordination sphere of *Tt*-Cu_A by those from a homologous eukaryotic domain (*Tt*-3L variant).[12] $\Delta E_{\sigma_u^*/\pi_u}$ values for native *Tt*-Cu_A, M160H, M160Q and the *Tt*-3L variants are 600, 200, 900, and 240 cm^{-1}, respectively.[10,12] Thus, the populations of the π_u state at room temperature are 30–35% for M160H and *Tt*-3L, about 5% for WT *Tt*-Cu_A and about 1% for M160Q. One can anticipate that for sufficiently large $\Delta E_{\sigma_u^*/\pi_u}$, displacement along the ET reaction coordinate is likely to proceed through the lower lying σ_u^* GS. Smaller gaps, in contrast, may lead to ET exclusively from the π_u GS. The underlying idea, as shown by QM calculations,[10] is that a variety of small structural distortions result in an adiabatic $\sigma_u^* \rightarrow \pi_u$ transition. If the reaction coordinates for this transition and for ET are coupled, the π_u GS may become redox active and ET through the σ_u^* GS is disabled, even if this GS remains energetically lower (see Figure S1 in the Supporting Information). In such scenario, the relative magnitudes of the $\Delta E_{\sigma_u^*/\pi_u}$ versus the ET activation free energy ($\Delta G^{\ddagger}$) determine the redox-active GS. Indeed, first and second sphere mutants of Cu_A have been shown to present either σ_u^* or π_u redox-active GSs, depending on the magnitude of their $\Delta E_{\sigma_u^*/\pi_u}$.[10,12] Here we report that a reversible functional switching between a σ_u^* and a π_u redox-active GSs can be elicited by pH changes within the same protein variant. The combined use of electrochemical and spectroscopic techniques to assess this unique behavior unveils differences in electronic coupling for both states and further supports the feasibility of an in vivo regulatory mechanism by this switching.

[*] U. Zitare,[+] Dr. D. Alvarez-Paggi,[+] Prof. D. H. Murgida
Instituto de Química Física de los Materiales
Medio Ambiente y Energía
Departamento de Química Inorgánica
Analítica y Química Física
Facultad de Ciencias Exactas y Naturales
Universidad de Buenos Aires and CONICET (Argentina)
E-mail: dhmurgida@qi.fcen.uba.ar
M. N. Morgada, Dr. L. A. Abriata, Prof. A. J. Vila
Instituto de Biología Molecular y Celular de Rosario (IBR)
Departamento de Química Biológica
Facultad de Ciencias Bioquímicas y Farmacéuticas
Universidad Nacional de Rosario and CONICET (Argentina)
[+] These authors contributed equally to this work.

[**] We thank CONICET, ANPCyT, and UBACYT for funding.
Supporting information for this article is available on the WWW under http://dx.doi.org/10.1002/anie.201504188.

Protein samples were adsorbed on Au electrodes coated with self-assembled monolayers (SAMs) to produce relatively well oriented protein films,[13] and were functionally assessed by cyclic voltammetry (CV). This method was chosen instead of solution electrochemistry to bypass protein diffusion that hampers comparative kinetic studies between the different protein variants, particularly regarding electronic couplings. The reduction potentials obtained in solution and for the protein films are very similar, thereby indicating that the structure of the different Cu_A sites is preserved upon adsorption (Table S1).

Rate constants of heterogeneous ET at zero driving force (k_{ET}; $\Delta G^\circ = 0$) were obtained using Laviron's working curve[14] (Figures S2–S5) and ET activation enthalpies, $\Delta H^{\neq}$ were estimated from Arrhenius plots in the temperature range 5–40 °C using a nonisothermal cell. Simple Boltzmann considerations show that the σ_u^*/π_u relative populations do not change significantly within this range (Figure S6). Considering that the entropic contribution in redox proteins is usually very small,[15] one can approximate $\Delta H^{\neq} \approx \Delta G^{\neq} = \lambda/4$ for $\Delta G^\circ = 0$.[16]

As shown in Figure 1 and S7, we observe a pH-dependent transition of k_{ET} for M160H with a p*K*a of about 5.0 and a two-fold increase from low to high pH values. This is paralleled by a transition of the activation parameters. At low pH we obtain $\lambda = 0.34$ eV ($\Delta H^{\neq} = 8.2$ kJ mol^{-1}), a value similar to those reported for *Tt*-Cu_A and M160Q, with a σ_u^* redox-active GS.[10] At high pH, instead, the measured values ($\lambda = 0.60$ eV, $\Delta H^{\neq} = 15.5$ kJ mol^{-1}) are similar to *Tt*-3L, a variant with a π_u GS,[12] thus suggesting a σ_u^*/π_u transition. These results may appear to contradict ET theory at first glance. Upon activation of the π_u GS as the redox-active one, k_{ET} is expected to decrease due to its higher λ value. In fact, Gorelsky and coworkers proposed a larger λ value in the π_u GS rendering it inefficient for ET.[9] Surprisingly, we observe the opposite trend for the M160H mutant, that is, the pH-dependent increase of λ concurs with an unexpected rise of k_{ET}. In the context of Marcus theory, this observation can only be rationalized in terms of a about 7.5-fold enhancement of the electronic coupling towards the metal electrode that overrides the larger λ. The observed transition is fully reversible with pH (Figure 1). Moreover, from the peak areas of the CVs, it is estimated that less than 10% of the adsorbed protein is lost during the process of changing pH back and forward.

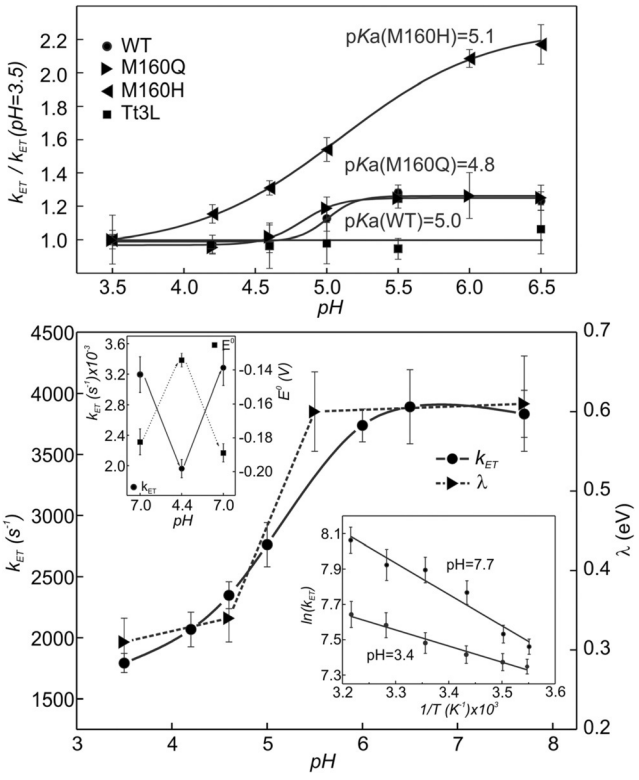

Figure 1. A) Variation of k_{ET} as a function of pH. The values shown are normalized by k_{ET} at pH 3.5. B) Increase of k_{ET} and λ as a function of pH for M160H. Inset 1: Reversibility of the pH-induced changes on E° and k_{ET}. Inset 2: Arrhenius plots at pH 3.4 and 7.7 from which λ is obtained.

The k_{ET} values for WT and M160Q are almost identical, and both exhibit a small variation with pH of about 20%. This indicates that the single point mutation of the internal residue M160 exerts no appreciable effect on the protein/SAM interactions. The activation parameters of WT *Tt*-Cu_A and M160Q are also identical ($\lambda = 0.29$ eV; $\Delta H^{\neq} = 7.0$ kJ mol^{-1}), independent of pH and consistent with the value expected for a σ_u^* GS.[9,10,17] While small rearrangements of protein and interfacial water molecules can account for the mild pH kinetic effect observed for WT and M160Q,[18,19] they cannot explain the much larger effect observed for M160H. First one has to consider that the structure and main spectroscopic features are largely preserved upon mutation, as determined by UV/Vis, NMR, RR, EXAFS, EPR, and QM/MM calculations.[10,20] Second and most important, reorientation effects are not expected to produce a two-fold increase of λ, as observed for M160H. Therefore we conclude that the enhanced coupling observed in M160H at high pH arises from the activation of the π_u GS, which exhibits a different electronic density distribution compared to the σ_u^* GS, as suggested by previous pathways and QM calculations and NMR experiments.[10] In contrast, the small variation of k_{ET} for WT and M160Q is most likely the result of minor reorientations due to protonation/deprotonation of surface residues at the protein/SAM binding site, consistent with the pH-dependence of the SPR signals (Figure S8). The results obtained for *Tt*-3L are in good agreement with this interpretation. In this variant the 3 loops that constitute the putative binding site to the SAM are mutated, exhibiting slightly higher and pH insensitive k_{ET}, which probably denotes a marginally different coarse orientation in the adsorbed state. The activation parameters of *Tt*-3L are insensitive to pH and are in the range reported for a π_u redox-active molecular orbital ($\lambda = 0.60$ eV; $\Delta H^{\neq} = 15.5$ kJ mol^{-1}).[12]

In order to unveil whether the alternation of the active GS could account for the observed electrochemical response, we studied the effect of pH on the different protein variants in solution by UV/Vis, resonance Raman (RR), EPR, and NMR spectroscopy. For the mixed-valence WT and M160Q variants, the UV/Vis spectra are dominated by two intense $S_{Cys} \rightarrow Cu$ charge transfer (CT) bands at 21270 and 18700 cm^{-1}, $N_{His} \rightarrow$

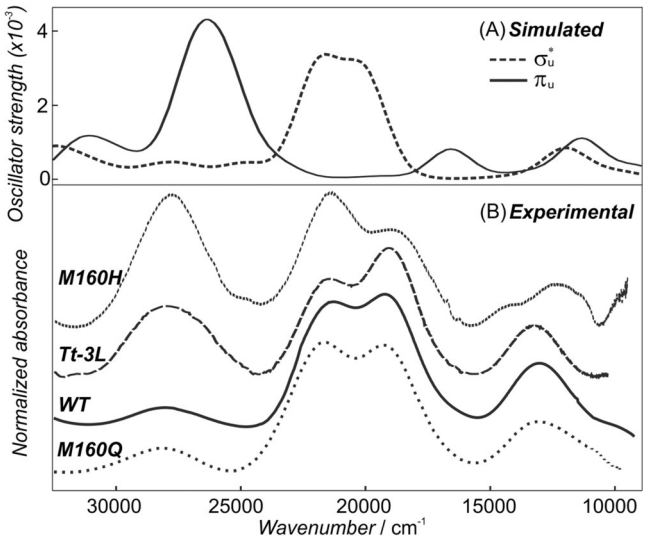

Figure 2. A) TD-DFT calculations of the oscillator strength for the electronic transitions of σ_u^* and π_u GSs of Cu_A centers. B) Experimental UV/Vis spectra of WT, M160Q, Tt-3L-Cu_A and M160H acquired at pH 7 and 25 °C.

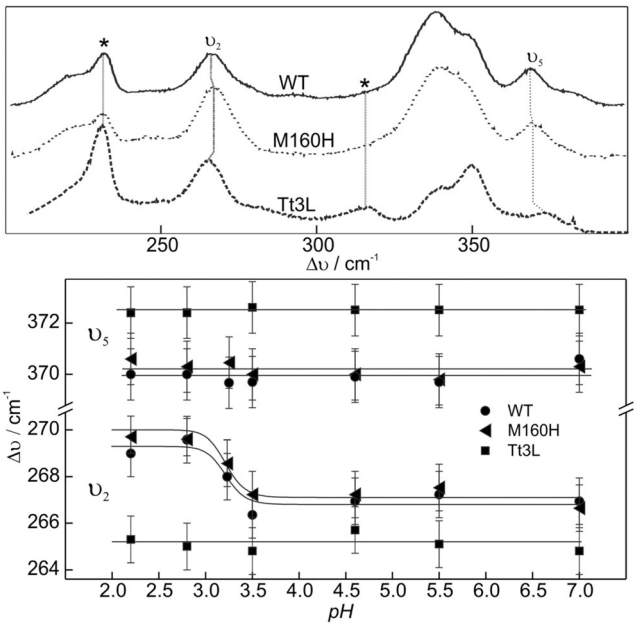

Figure 3. Top: RR spectra acquired with 514 nm excitation at pH 5.5 for Cu_A WT, *Tt*-3L and M160H. Bottom: pH dependency of the ν_2 and ν_5 bands for the studied species. WT and M160H exhibit a transition with an apparent p*K*a of 3.2 for ν_2, while for *Tt*-3L it remains constant within experimental error.

Cu CT transitions at 28000 and 25800 cm^{-1} and a $\psi \rightarrow \psi^*$ intervalence band at 12650 cm^{-1} (Figure 2). These features correspond to a σ_u^* GS, as previously determined from TD-DFT calculations.[10] These calculations also show that the UV/Vis spectrum of the π_u GS is characterized by a blue shift of the $S_{Cys} \rightarrow Cu$ band to about 28000 cm^{-1}, partially overlapping with the $N_{His} \rightarrow Cu$ transitions, whereas the intervalence band appears at 12100 cm^{-1}.[10] In the M160H and *Tt*-3L mutants, due to the higher population of the π_u state, the UV/Vis spectra are a convolution of the spectroscopic features of both GS (Figure 2). The intensity ratio of the CT bands at 28000 and 18500 cm^{-1} provides an estimate of the σ_u^*/π_u relative populations that, as shown in Figure S9, correlate well with the $\Delta E_{\sigma_u^*/\pi_u}$ values obtained by NMR.

The RR spectra of WT *Tt*-Cu_A, M160Q and M160H acquired under 514 nm excitation, that is, in resonance with the $S_{Cys} \rightarrow Cu$ CT of the σ_u^* GS, are all very similar, while *Tt*-3L presents some small differences (Figure 3 and Figure S10). In all cases they are dominated by normal modes arising from distortions of the Cu_2S_2 diamond core.[21,22] Interestingly, the position of the ν_2 band (ca. 260 cm^{-1}) of WT, M160H and M160Q is slightly sensitive to pH and exhibits an apparent p*K*a of 3.1, while for *Tt*-3L the spectra are pH-independent. This is in agreement with our recent report of an acid-base transition in WT *Tt*-Cu_A with a p*K*a of 3.5 attributed to a small pH-induced effect in the protein matrix, which does not impact on the σ_u^*/π_u populations but affects the rate of proton exchange of the equatorial ligand H157.[23] Remarkably, the ν_2 band corresponds to an A_{1g} vibrational mode that presents significant contributions of Cu–N, Cu–S and Cu–Cu stretching[21,22] and, therefore, is expected to be sensitive to perturbations in H157 through the Cu-N stretching component. Given that the 514 nm laser line selectively excites the σ_u^* GS, the observed changes do not directly reflect changes of σ_u^*/π_u populations. Instead, they are most likely related to subtle perturbations of the site in the σ_u^* GS, which in turn may affect the size of the energy gap in M160H (see below). Consistently, the band ν_5 (ca. 360 cm^{-1}), which corresponds to a normal mode involving almost exclusively the Cu and S atoms that are not solvent exposed, is not affected by pH in any protein variant (Figure 3 and Figure S10). The fact that the RR spectra of the σ_u^* GS for all the protein variants are very similar and vary only slightly with pH for M160H do not allow to describe the changes in the ET rates based on the assumption of a perturbed σ_u^* state. Indeed, a perturbation of the σ_u^* GS eliciting a two-fold increase of λ is expected to result in about 10 cm^{-1} upshift of most RR bands that is not observed in the present study.[24] We are then left with the possibility that the π_u GS is the redox-active state in the M160H mutant at high pH.

In contrast to the other variants, the electronic absorption spectrum of M160H varies with pH (Figure 4 and S11). Specifically, we observe a reversible variation of the 28000 cm^{-1}/18500 cm^{-1} relative intensities. The temperature dependencies of the UV/Vis spectra at pH 2.4 and 7, that is, before and after the transition revealed by RR spectroscopy, show that the population of the π_u state increases with pH, thus suggesting a about 25% smaller σ_u^*/π_u energy gap that, according to the electrochemical response, is sufficient to render the π_u GS as the only redox active at high pH, and *vice versa*. EPR spectra show that the $g_\parallel$ value is lowered from 2.219 to 2.210 at low pH, while the mixed valence features are preserved (Figure S12 and Table S2). This change can be interpreted as an increase in the energy gap for the vertical transition from the σ_u^* GS to the π_u excited state (Table S2). These results prompted us to study the energy gap between both GSs by NMR spectroscopy, which (despite being challenging under these extreme pH conditions) is the most

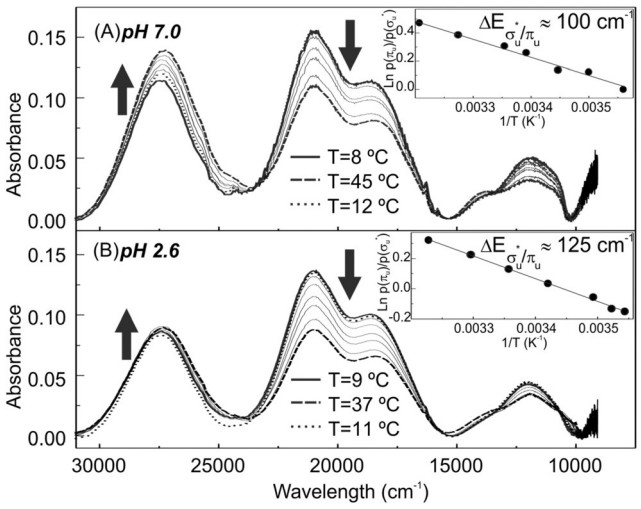

Figure 4. Top: UV/Vis spectra of M160H at pH 7.0 (A) and 2.6 (B) at increasing temperatures. After obtaining spectra at the maximum temperatures, the samples were cooled down to acquire new spectra and rule out protein denaturing. Insets: σ_u^*/π_u populations and energy gaps obtained from the ratio of the S_{Cys} CT bands at 28000 cm^{-1}/ 18500 cm^{-1}as a function of temperature.

adequate technique for this purpose. ^{1}H NMR spectra show perturbed chemical shifts for the four β Cys protons at pH 2.5. The observed shift perturbation at low pH faithfully reproduces that induced by temperature changes that correspond to a larger population of the σ_u^* (Figure S13), that is consistent with a larger energy gap between the two GS at low pH.

Overall, UV/Vis, EPR, and NMR spectroscopy concur in supporting a larger population of the π_u state at high pH in variant M160H. On the other hand, RR shows that there are no perturbations of the σ_u^* state induced by pH changes, allowing us to rule out the existence of a conversion from a symmetric to an asymmetric mixed valence σ_u^* state, as reported for an artificial Cu_A site engineered into the blue copper protein azurin (Azu-Cu_A).[24–26] Such a conversion involves distinct changes of the vibrational and electronic spectra and a about 150 mV up-shift of the formal potential, that are not observed in the present work. Notably, the energy gap of *Tt*-3L is as small as for the M160H mutant, but in this case the UV/Vis and RR spectra are pH-independent. Apparently, substitution of the three loops necessary to create *Tt*-3L, which results in replacement of L155, G156, and Q158 in the vicinity of H157, alters the metal site environment to render it insensitive to pH in the studied range.[12]

Both the electrochemical and spectroscopic results are consistent with an acid-base equilibrium that modulates the $\Delta E_{\sigma_u^*/\pi_u}$ value of M160H. The apparent p*K*as obtained for the adsorbed proteins, however, are upshifted relative to solution values. This is not unexpected as, most likely, it reflects differences of local pH, dielectric constants, and solvent accessibilities of relevant amino acids in the two experimental situations.[27–29] Indeed, we determined a similar apparent upshift of the isoelectric point of Cu_A upon adsorption that reveals a lower interfacial pH compared to the bulk solution (Figure S14).

In summary, we present compelling evidence of what, to the best of our knowledge, constitutes the first example of a (biological) redox center that can undergo pathways switching resulting from the reversible activation of two alternative ground states. Compared with recent reports from our group,[10,12] here we have been able to probe the redox properties of the two states in the same molecular species, the M160H mutant of *Tt*-Cu_A. The switching could not be directly observed for the WT protein with the present experimental approach, presumably due to the larger $\Delta E_{\sigma_u^*/\pi_u}$ that appears to render it insensitive to pH variations. However, DFT calculations indicate that the nearly degenerate states may be populated with minimal structural perturbations.[10] Moreover, the present results show that both states are redox active and capable of participating in heterogeneous ET reactions with comparable efficiency. The increase of k_{ET} for the π_u state in spite of the higher reorganization energy suggests that, as a consequence of the GS switching, the preferred electronic pathways are alternated due to redistribution of the electronic density. This hypothesis has been challenged on the basis of theoretical and spectroscopic results for Azu-Cu_A.[30] This model system has proven very useful for studying structural, electronic and redox features of the Cu_A site, as it constituted one of the few robust and accessible Cu_A centers.[9,24,25,31–34] Recent investigations, however, demonstrated that several properties, including energy gap modulation and pH susceptibility, are markedly different between native and engineered Cu_A sites.[20,23] Certainly, the study of native and engineered sites provides complementary views of this dinuclear site.

The finding that both GS can actually be redox active in the same protein variant strongly suggests that their thermal equilibrium may constitute the basis of the puzzling efficiency and directionality of electron entry and exit in Cu_A sites, as the enhanced superexchange coupling of the π_u state may render it suitable for participating in the ET reaction, even if poorly populated.[10] In addition, it puts forward the idea that the features of the *Tt*-Cu_A site, namely its stability and transistor-like properties for the ET reaction, may be exploited for the development of protein-based molecular electronic devices.

Experimental Section

Protein preparation: WT and mutant Cu_A-soluble fragments from subunit II of the cytochrome ba_3 from *T. thermophilus* were produced as described previously[35,36] and stored in 100 mM phosphate buffer (pH 6.0; 100 mM KCl).

Electronic absorption spectra: UV/Vis spectra were acquired with a Thermo Scientific Evolution Array spectrophotometer employing 1 cm or 0.1 cm path length as required. Measurements were performed in either a 10 mM acetate buffer (500 mM KNO_3) or 10 mM phosphate buffer (200 mM KNO_3) as required.

Resonance Raman spectroscopy: RR spectra were acquired in backscattering geometry by using Jobin Yvon XY 800 Raman microscope equipped with a CCD detector. See the Supporting Information for further details.

Cyclic voltammetry: CV experiments were performed with a Gamry REF600 potentiostat using a water jacketed non-isothermal cell contained into a Faraday cage (Vista Shield). See the Supporting Information for further details.

NMR spectroscopy: NMR experiments were carried out on a Bruker Avance II Spectrometer operating at 600.13 MHz (^{1}H frequency). See the Supporting information for further details.

EPR spectroscopy: X-band CW-EPR measurements were performed on a Bruker EMX-Plus spectrometer. See the Supporting Information for further details.

SPR spectroscopy: Surface Plasmon Resonance experiments were carried out using a SPR Navi 210A instrument at 670 nm. See the Supporting Information for further details.

Keywords: cytochrome *c* oxidase · electrochemistry · electronic structures · electron transfer · enzymes

How to cite: *Angew. Chem. Int. Ed.* **2015**, *54*, 9555 – 9559
Angew. Chem. **2015**, *127*, 9691 – 9695

[1] H. B. Gray, J. R. Winkler, *Annu. Rev. Biochem.* **1996**, *65*, 537 – 561.
[2] S. S. Skourtis, D. H. Waldeck, D. N. Beratan, *Annu. Rev. Phys. Chem.* **2010**, *61*, 461 – 485.
[3] S. S. Skourtis, I. A. Balabin, T. Kawatsu, D. N. Beratan, *Proc. Natl. Acad. Sci. USA* **2005**, *102*, 3552 – 3554.
[4] D. N. Beratan, J. N. Betts, J. N. Onuchic, *Science* **1991**, *252*, 1285 – 1288.
[5] I. A. Balabin, D. N. Beratan, S. S. Skourtis, *Phys. Rev. Lett.* **2008**, *101*, 158102 – 158106.
[6] D. Alvarez-Paggi, M. A. Castro, V. Tórtora, L. Castro, R. Radi, D. H. Murgida, *J. Am. Chem. Soc.* **2013**, *135*, 4389 – 4397.
[7] B. E. Ramirez, B. G. Malmström, J. R. Winkler, H. B. Gray, *Proc. Natl. Acad. Sci. USA* **1995**, *92*, 11949.
[8] P. A. Williams, N. J. Blackburn, D. Sanders, H. Bellamy, E. A. Stura, J. A. Fee, D. E. McRee, *Nat. Struct. Biol.* **1999**, *6*, 509 – 516.
[9] S. I. Gorelsky, X. Xie, Y. Chen, A. James, E. I. Solomon, *J. Am. Chem. Soc.* **2006**, *128*, 16452 – 16453.
[10] L. A. Abriata, D. Álvarez-Paggi, G. N. Ledesma, N. J. Blackburn, A. J. Vila, D. H. Murgida, *Proc. Natl. Acad. Sci. USA* **2012**, *109*, 17348 – 17353.
[11] L. A. Abriata, G. N. Ledesma, R. Pierattelli, A. J. Vila, *J. Am. Chem. Soc.* **2009**, *131*, 1939 – 1946.
[12] M. N. Morgada, L. A. Abriata, U. Zitare, D. Alvarez-Paggi, D. H. Murgida, A. J. Vila, *Angew. Chem.* **2014**, *126*, 6302 – 6306.
[13] K. Fujita, N. Nakamura, H. Ohno, B. S. Leigh, K. Niki, H. B. Gray, J. H. Richards, *J. Am. Chem. Soc.* **2004**, *126*, 13954 – 13961.
[14] E. Laviron, *J. Electroanal. Chem. Interface* **1979**, *101*, 19 – 28.
[15] A. A. Milischuk, D. V. Matyushov, M. D. Newton, *Chem. Phys.* **2006**, *324*, 172 – 194.
[16] R. A. Marcus, N. Sutin, *Biochim. Biophys. Acta* **1985**, *811*, 265 – 322.
[17] M. H. M. Olsson, U. Ryde, *J. Am. Chem. Soc.* **2001**, *123*, 7866 – 7876.
[18] D. Alvarez-Paggi, D. F. Martin, P. M. DeBiase, P. Hildebrandt, M. A. Marti, D. H. Murgida, *J. Am. Chem. Soc.* **2010**, *132*, 5769 – 5778.
[19] D. A. Paggi, D. F. Martin, A. Kranich, P. Hildebrandt, M. A. Martí, D. H. Murgida, *Electrochim. Acta* **2009**, *54*, 4963 – 4970.
[20] G. N. Ledesma, D. H. Murgida, H. K. Ly, H. Wackerbarth, J. Ulstrup, A. J. Costa-Filho, A. J. Vila, *J. Am. Chem. Soc.* **2007**, *129*, 11884 – 11885.
[21] C. R. Andrew, R. Fraczkiewicz, R. S. Czernuszewicz, P. Lappalainen, M. Saraste, J. Sanders-Loehr, *J. Am. Chem. Soc.* **1996**, *118*, 10436 – 10445.
[22] D. R. Gamelin, D. W. Randall, M. T. Hay, R. P. Houser, T. C. Mulder, G. W. Canters, S. de Vries, W. B. Tolman, Y. Lu, E. I. Solomon, *J. Am. Chem. Soc.* **1998**, *120*, 5246 – 5263.
[23] D. Alvarez-Paggi, L. A. Abriata, D. H. Murgida, A. J. Vila, *Chem. Commun.* **2013**, *49*, 5381 – 5383.
[24] X. Xie, S. I. Gorelsky, R. Sarangi, D. K. Garner, H. J. Hwang, K. O. Hodgson, B. Hedman, Y. Lu, E. I. Solomon, *J. Am. Chem. Soc.* **2008**, *130*, 5194 – 5205.
[25] H. J. Hwang, Y. Lu, *Proc. Natl. Acad. Sci. USA* **2004**, *101*, 12842 – 12847.
[26] D. Lukoyanov, S. M. Berry, Y. Lu, W. E. Antholine, C. P. Scholes, *Biophys. J.* **2002**, *82*, 2758 – 2766.
[27] M. Rooth, A. M. Shaw, *Phys. Chem. Chem. Phys.* **2006**, *8*, 4741 – 4743.
[28] W. Sanders, R. Vargas, M. R. Anderson, *Langmuir* **2008**, *24*, 6133 – 6139.
[29] D. H. Murgida, P. Hildebrandt, *J. Phys. Chem. B* **2001**, *105*, 1578 – 1586.
[30] M. L. Tsai, R. G. Hadt, N. M. Marshall, T. D. Wilson, Y. Lu, E. I. Solomon, *Proc. Natl. Acad. Sci. USA* **2013**, *110*, 14658 – 14663.
[31] M. Hay, J. H. Richards, Y. Lu, *Proc. Natl. Acad. Sci. USA* **1996**, *93*, 461 – 464.
[32] M. T. Hay, M. C. Ang, D. R. Gamelin, E. I. Solomon, W. E. Antholine, M. Ralle, N. J. Blackburn, P. D. Massey, X. Wang, A. H. Kwon, *Inorg. Chem.* **1998**, *37*, 191 – 198.
[33] H. J. Hwang, S. M. Berry, M. J. Nilges, Y. Lu, *J. Am. Chem. Soc.* **2005**, *127*, 7274 – 7275.
[34] M. G. Savelieff, Y. Lu, *Inorg. Chim. Acta* **2008**, *361*, 1087 – 1094.
[35] C. O. Fernández, J. A. Cricco, C. E. Slutter, J. H. Richards, H. B. Gray, A. J. Vila, *J. Am. Chem. Soc.* **2001**, *123*, 11678 – 11685.
[36] C. E. Slutter, D. Sanders, P. Wittung, B. G. Malmström, R. Aasa, J. H. Richards, H. B. Gray, A. James, *Biochemistry* **1996**, *35*, 3387 – 3395.

Received: May 7, 2015
Published online: June 26, 2015

Angewandte Chemie
Eine Zeitschrift der Gesellschaft Deutscher Chemiker

Supporting Information

Reversible Switching of Redox-Active Molecular Orbitals and Electron Transfer Pathways in Cu_A Sites of Cytochrome *c* Oxidase**

*Ulises Zitare, Damián Alvarez-Paggi, Marcos N. Morgada, Luciano A. Abriata, Alejandro J. Vila, and Daniel H. Murgida**

anie_201504188_sm_miscellaneous_information.pdf

Supporting Information

Experimental Section

Cyclic Voltammetry. The electrochemical cell was equipped with a polycrystalline gold bead working electrode, a Pt wire auxiliary electrode and a Ag/AgCl (3.5 M KCl) reference electrode to which all potentials in this work are referred. Measurements were performed employing the same electrolytes as for UV/Vis. Au electrodes were first oxidized in 10% $HClO_4$ applying a potential of 3 V for 2 minutes, sonicated in 10% HCl for 15 minutes, rinsed with water and subsequently treated with a 3:1 v/v H_2O_2 : H_2SO_4 mixture at 120 °C. The electrodes were then subjected to repetitive voltammetric cycles between -0.2 and 1.6 V in 10% $HClO_4$ and thoroughly washed with water and ethanol. Au working electrodes were coated with self-assembled monolayers (SAMs) by overnight incubation in an ethanolic 2mM HS-$(CH_2)_5$-CH_3 / 3mM HS-$(CH_2)_6$-OH solution. After thorough rinsing with ethanol and deionized water, the coated electrodes were incubated in a 100μM protein solution during 2 hours for protein adsorption and then transferred to the electrochemical cell. Measurements were performed in either a 10 mM acetate buffer/200mM KNO_3 buffer or 10 mM phosphate / 200mM KNO_3 buffer depending on the desired pH. The temperature was held fixed during measurements by controlling the temperature of a water jacket cell coupled to a circulating thermostat.

Resonance Raman. The 514 nm line (13 mW) of a cw argon laser (Coherent Innova 70c) was focused into 2 μL of frozen protein solution (77 K) contained in a Linkam THMS 300 thermostat. Spectra were acquired at 0.5 cm^{-1} resolution using the buffers described for UV/Vis.

NMR Spectroscopy. ^{1}H-detected spectra were acquired with a triple-resonance (TXI) probehead. ^{1}H spectra to for the observation of the broad Hβ signals were acquired with a SuperWEFT pulse sequence using a spectral window of ca. 360 kHz, and a total recycle delay of ca. 40 ms with variable intermediate delays. Protein samples for the experiments were prepared in phosphate buffer 100 mM pH6 with the addition of 100 mM KCl in 100% D_2O for assessing the temperature dependence. To assess the pH dependence, the pH was registered before and after recording the spectra. The samples were prepared in 100 mM Pi with the addition of 100mM KCl and the pH was lowered using a solution of citric acid, all in 100% D_2O.

EPR Spectroscopy. X-band CW-EPR measurements were performed on a Bruker EMX-Plus spectrometer equipped with a rectangular cavity and an Oxford Instruments continuous-flow cryostat. The experimental conditions were: microwave frequency, 9.4 GHz; microwave power, 2 mW; modulation amplitude, 4 G; field modulation, 100 kHz; temperature, 5K. EPR spectra were analyzed and simulated with the EasySpin toolbox based on MATLAB.[1] In a first approach, simulations were performed assuming a nearly axial g-tensor, anisotropic linewidths, and, since the spectra show no hyperfine structure, A-tensor components obtained from closely related systems characterized by ENDOR.[2;3] After this first approach, simulations were improved by adding both g- and A-strains until the best agreement with the experiment was obtained. Finally, the parameters so obtained were left to float within reasonable ranges using the routine esfit of EasySpin. pH dependent spectra were obtained on samples of *Tt*-CuA M160H in 50mM citrate buffer, 150mM KNO3 to mimic the conditions used in the electrochemistry measurements. The distinct pH were obtained adding 1M HCl to avoid high dilutions.

SPR Spectroscopy. Gold sensors (glass slides coated with ca. 48 nm of gold and ca. 2 nm of chromium, BioNavis Ltd, Tampere, Finland) were employed for SPR measurements at 670 nm. SPR sensors were cleaned by immersion in boiling NH_4OH (28%) /H_2O_2 (100 vol) 1:1 for 15 min and then rinsed with water and ethanol. Then, they were coated with self-assembled monolayers (SAMs) by overnight incubation in an ethanolic 2mM HS-$(CH_2)_5$-CH_3 / 3mM HS-$(CH_2)_6$-OH solution. Multi-Parametric (BioNavis Ltd, Tampere, Finland). Temperature was kept at 20°C. All SPR experiments were processed using the BioNavis Data viewer software.

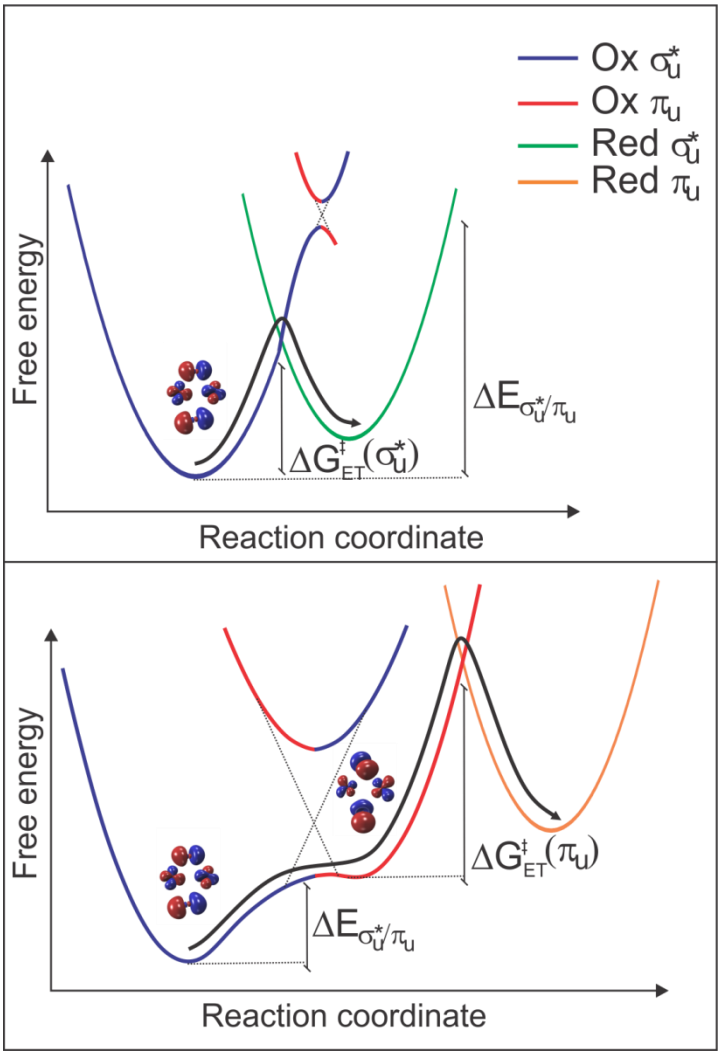

Figure S1. Model of the idealized potential energy surface for Cu_A centers that present a large energy gap ($\Delta E_{\sigma_u^*/\pi_u}$) such as WT and M160Q (top) or small $\Delta E_{\sigma_u^*/\pi_u}$, such as M160H at high pH and *Tt*-3L-CuA (bottom). The curves for the oxidized σ_u^* and π_u are shown in blue and red, while those for reduced σ_u^* and π_u are shown in green and orange, respectively. When $\Delta E_{\sigma_u^*/\pi_u}$ is large, the ET proceeds through the lower lying σ_u^* GS as expected. For M160H at high pH and *Tt*-3L-CuA, $\Delta G_{ET}^{\ddagger}(\sigma_u^*)$ is larger than $\Delta E_{\sigma_u^*/\pi_u}$. Thus, coupling of the reaction coordinates (RC) of the $\sigma_u^* \rightarrow \pi_u$ transition and the ET reaction in the σ_u^* GS abolishes the redox activity of the σ_u^* GS. Displacement through the ET RC results in a $\sigma_u^* \rightarrow \pi_u$ transition, and the ET reaction can only proceed through the π_u state. In consequence, the observable parameters of the ET reaction for these mutants, such as λ and H_{DA}, correspond to the π_u state. Although the reaction coordinate for the ET reaction is not known, we have shown that there are many RCs that yield a π_u GS.[4]

Table S1. Redox potentials (E^0) of the studied protein variants assessed by CV experiments in solution and of protein samples adsorbed on SAM-coated electrodes at varying pH values. A small upshift of *ca*. 30 mV of the E^0 values determined in solution with respect to the adsorbed proteins is observed, likely arising from the different dielectric constants of the electrolyte solution and the SAM coating, as well as differences of interfacial potential drops across the interfaces in the two experimental conditions.

Protein variant	E^0 (V) pH 7; solution CV	E^0 (V) pH 6.5; adsorbed CV	E^0 (V) pH 4.6; solution CV	E^0 (V) pH4.6; adsorbed CV
WT	0.055	0.034	0.072	0.064
M160H	-0.12	-0.145	-0.082	-0.107
M160Q	-0.108	-0.132	-0.043	-0.1

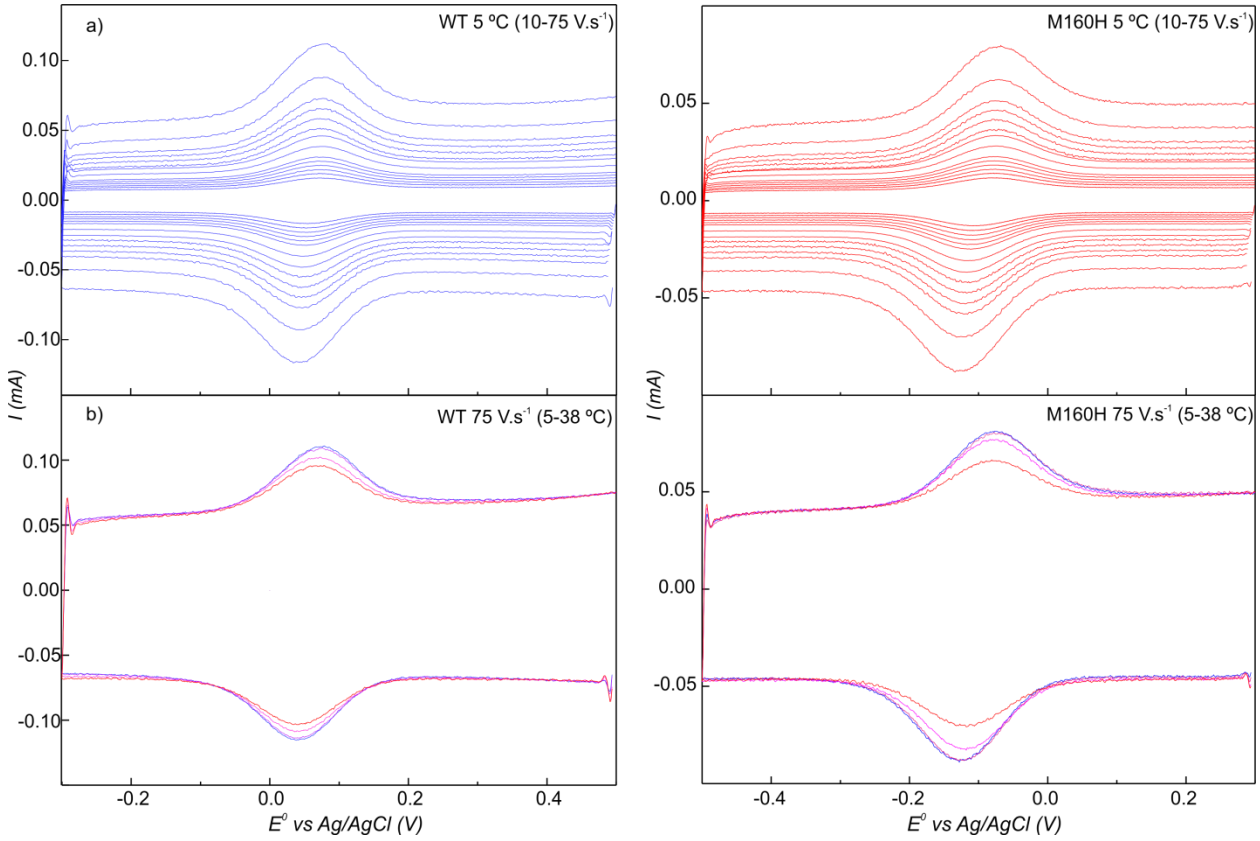

Figure S2. Cyclic voltammetries of *Tt*-CuA WT (left) and M160H (right) adsorbed on SAM-coated electrodes. The SAM composition is 2:3 HS-$(CH_2)_5$-CH_3:HS-$(CH_2)_6$-OH. Top: CVs acquired at 5 ºC at different scan rates. Bottom: CVs acquired at a scan rate of 75 $V.s^{-1}$ at different temperatures from 5 ºC to 38 ºC.

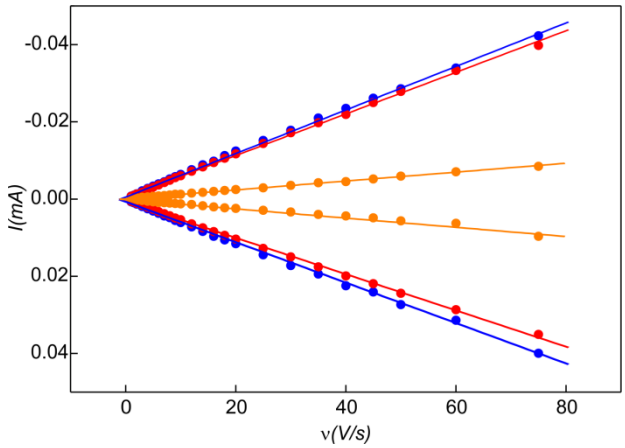

Figure S3. Peak current *vs* scan rate for *Tt*-CuA (blue), M160H (red) and *Tt*-3L-CuA (orange) from CVs of protein samples adsorbed on SAM-coated electrodes at 25 ºC and pH 4.6. The linear dependency is indicative of the redox activity characteristic of adsorbed species.

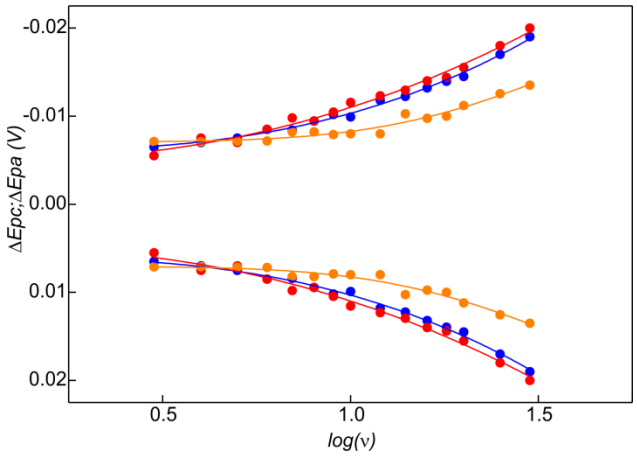

Figure S4. Trumpet plots of anodic and cathodic peak potentials for *Tt*-CuA (blue), M160H (red) and *Tt*-3L-CuA (orange) from CVs of protein samples adsorbed on SAM-coated electrodes at 5 ºC and pH 5.5. From these plots the apparent k_{ET} was estimated using Laviron's working curve.

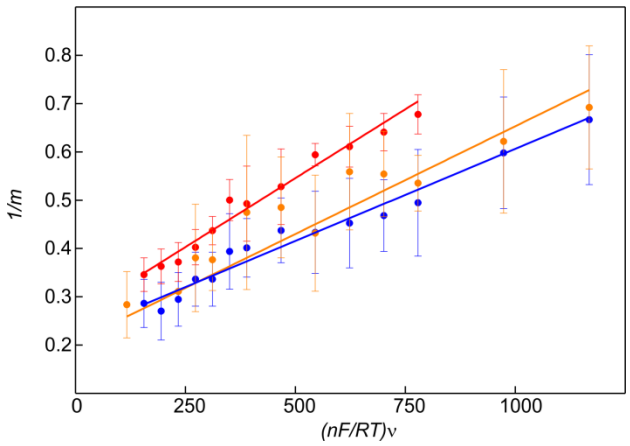

Figure S5. Laviron's working curves obtained for determining k_{ET} values for *Tt*-CuA (blue), M160H (red) and *Tt*-3L-CuA (orange) adsorbed on SAM-coated electrodes at pH 4.6 and 25 ºC. Laviron's formalism allows to determine k_{ET} of adsorbed species by evaluating the peak separation as a function of scan rate in cyclic voltammetries for separations of the anodic and cathodic peaks of up to 200 mV.[5] The working curve is valid for $0.3 < \alpha < 0.7$, which is suitable for our CVs considering the symmetric peaks of the voltagrams. Laviron's working curve rests on the Butler-Volmer formalism, that for small peak separations is equivalent to Marcus theory of electron transfer accounting for the electronic density of states in the metal electrode.[6]

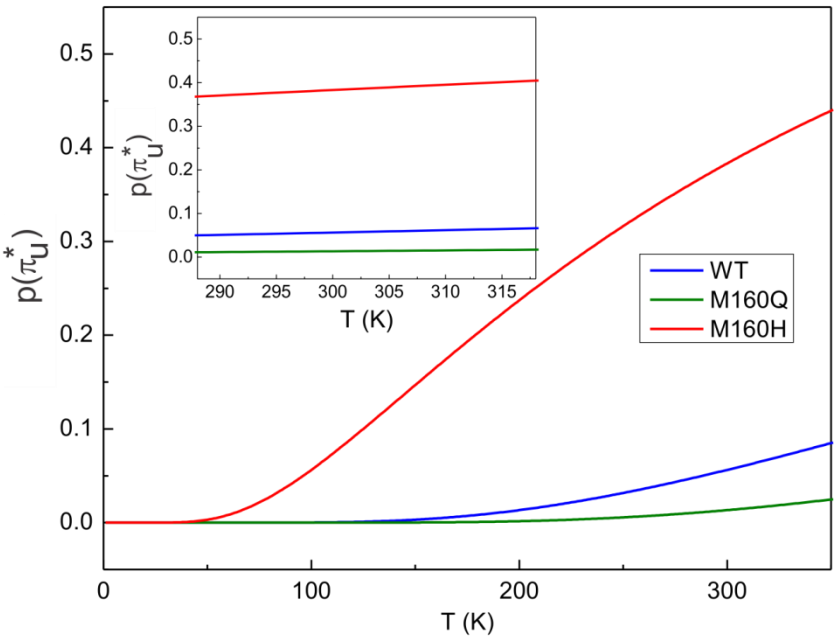

Figure S6. Population of the π_u electronic state in Cu_A WT (blue), M160Q (green) and M160H (red) from 0K to 350K, estimated from Boltzmann equation using $\Delta E_{\sigma_u^*/\pi_u}$ values obtained by paramagnetic NMR. Inset: Population of the π_u ground state in the temperature range of electrochemical determinations, where it remains practically constant.

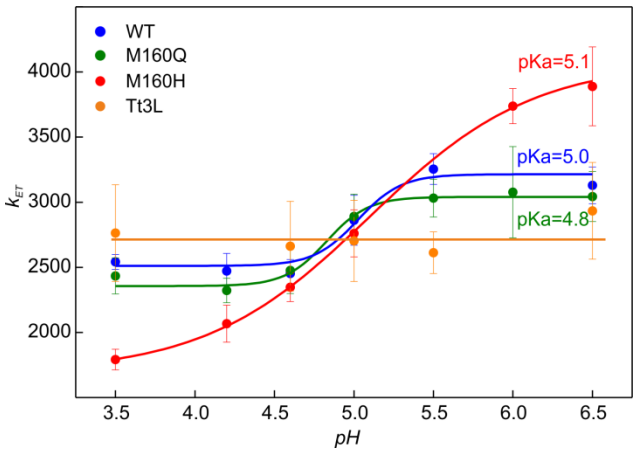

Figure S7. k_{ET} as a function of pH for *Tt*-CuA (blue), M160H (red) M160Q (green) and *Tt*-3L-CuA (orange) adsorbed on SAM-coated electrodes at 25 ºC. All the observed transitions present a similar apparent p*K*a value, except for the *Tt*-3L-CuA variant that remains nearly constant.

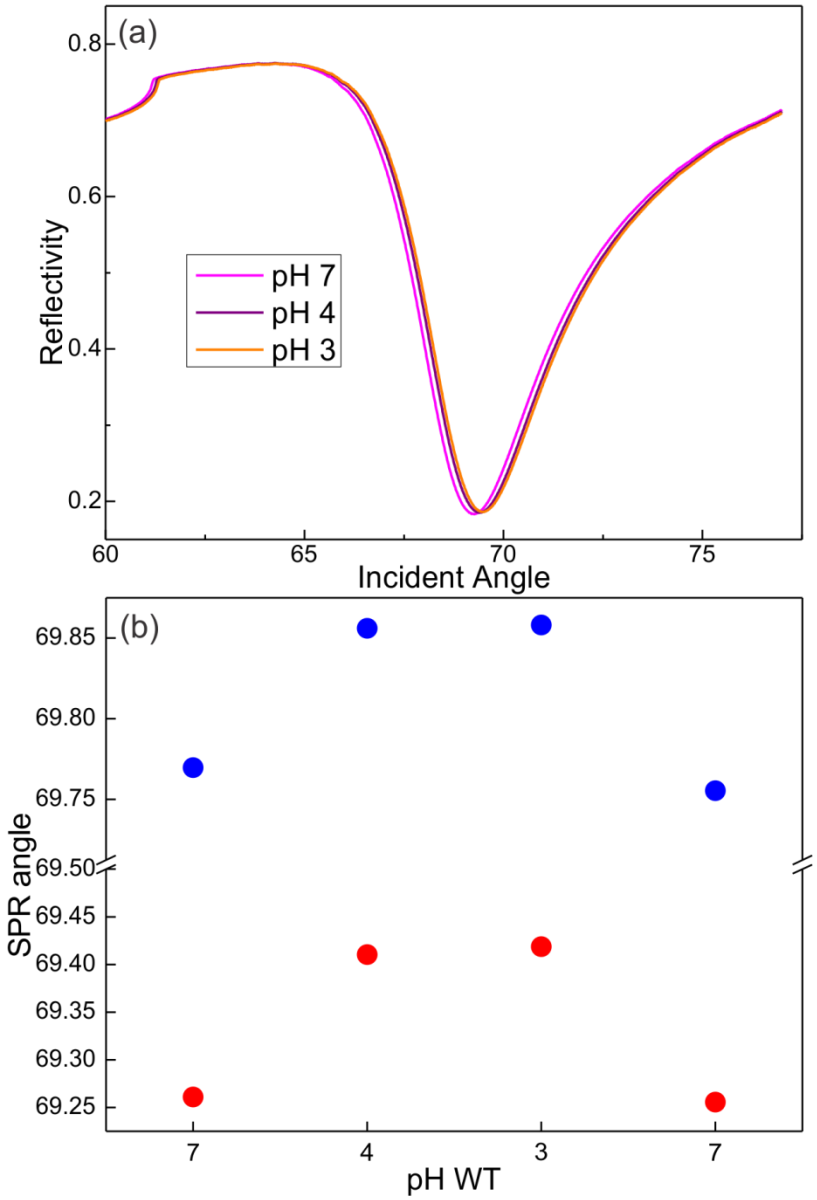

Figure S8. (a) SPR curves acquired for M160H adsorbed on a SAM-coated gold substrate at pH 3, 4 and 7. (b) SPR angle for WT-CuA (blue) and M160H (red) at varying pH values. The initial solution pH was 7, which was subsequently lowered to 4 and 3, before returning to the initial value of 7 to check for reversibility. The changes in the SPR angle are indicative of a reversible protein reorientation which is similar for both protein samples.

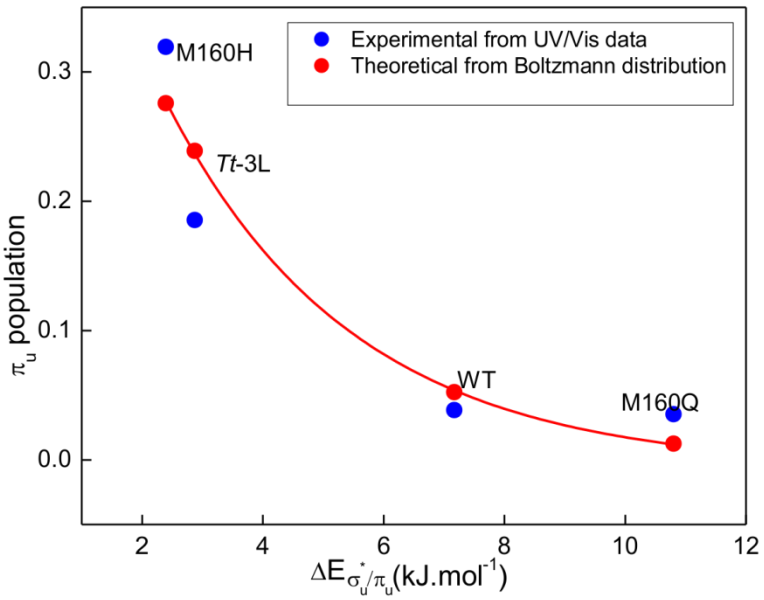

Figure S9. Blue: Population of the π_u electronic state assessed from the UV/Vis spectra as a function of the energy gaps determined by NMR. Red: populations of the π_u state obtained from the Boltzmann analysis of the NMR-determined gaps (red). The populations assessed from UV/Vis spectra were calculated from the intensities of the S_{Cys}-Cu CT in the π_u state and σ_u^* states taking into account that a) TD-DFT calculations show that the S_{Cys}-Cu CT band at ~380 nm, characteristic of the π_u state, presents a molar absorptivity 33% higher than that of the corresponding transition in the σ_u^* state (Figures S10) and b) the π_u S_{Cys}-Cu CT band overlaps with the σ_u^* N_{His}-Cu CT band whose molar absorptivity is *ca.* 32% of the S_{Cys}-Cu CT in the σ_u^* electronic state as observed in the spectra of the M160Q variant for which the population of the π_u is negligible small (<1%).

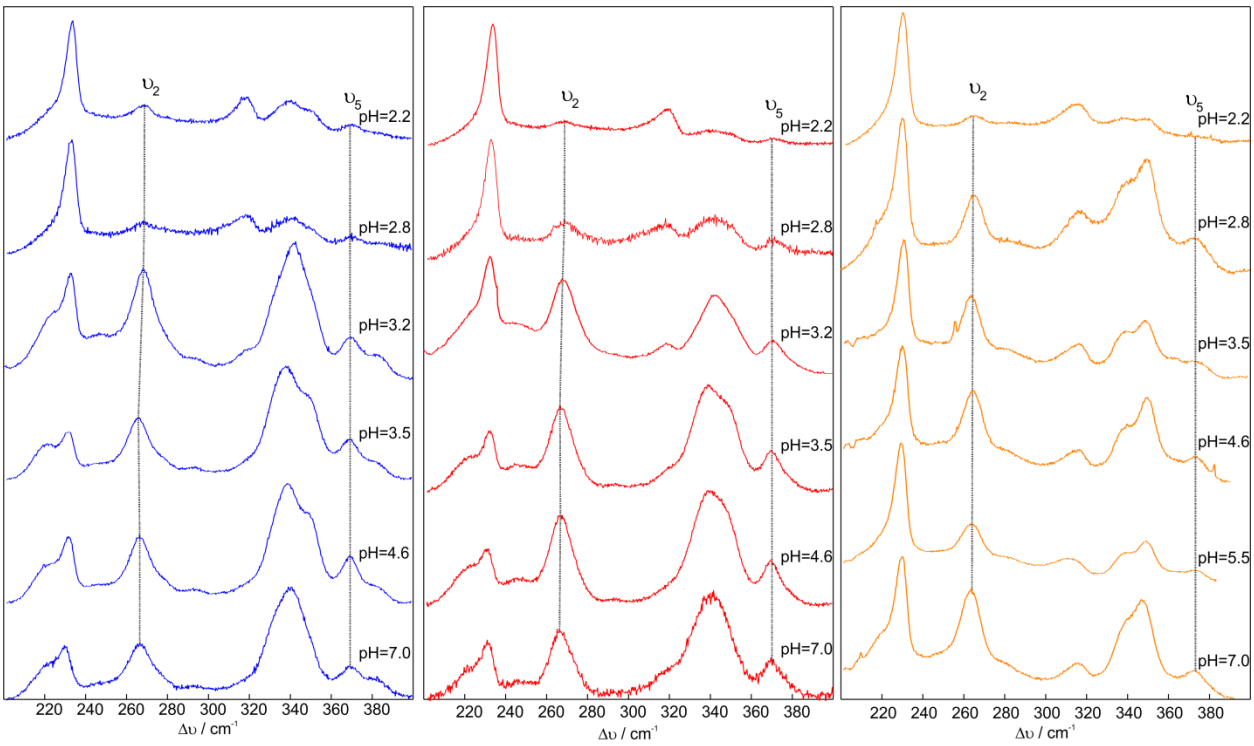

Figure S10. Resonance Raman spectra as function of pH for *Tt*-CuA (blue), M160H (red) and *Tt*-3L-CuA (orange). All measurements were obtained with 514nm laser excitation and with samples freezed at -190 ºC. The υ_2 band exhibits a weak pH dependence while the position of υ_5 remains unchanged in the entire pH range.

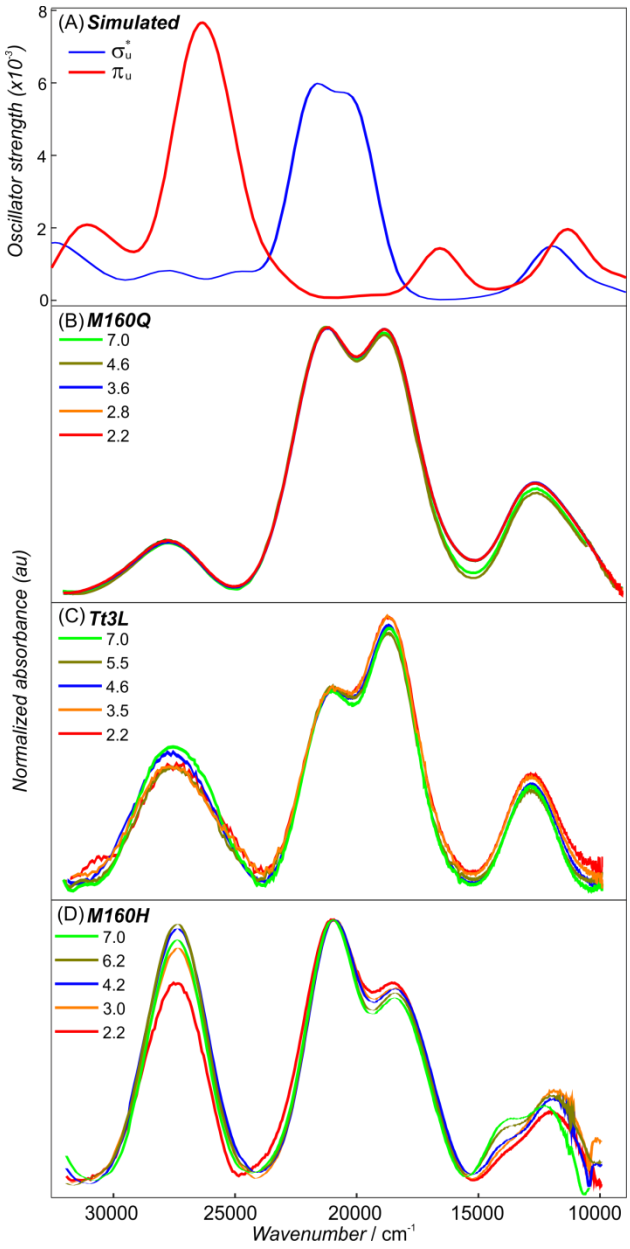

Figure S11. TD-DFT calculations of the oscillator strength for the electronic transitions of σ_u^* (blue) and π_u(red) GS of Cu_A centers (A). Experimental UV/Vis spectra of M160Q (B) *Tt*-3L-CuA (C) and M160H (D) at varying pH normalized by the absorbance of the ~21300 cm^{-1} S_{Cys}→Cu CT band.

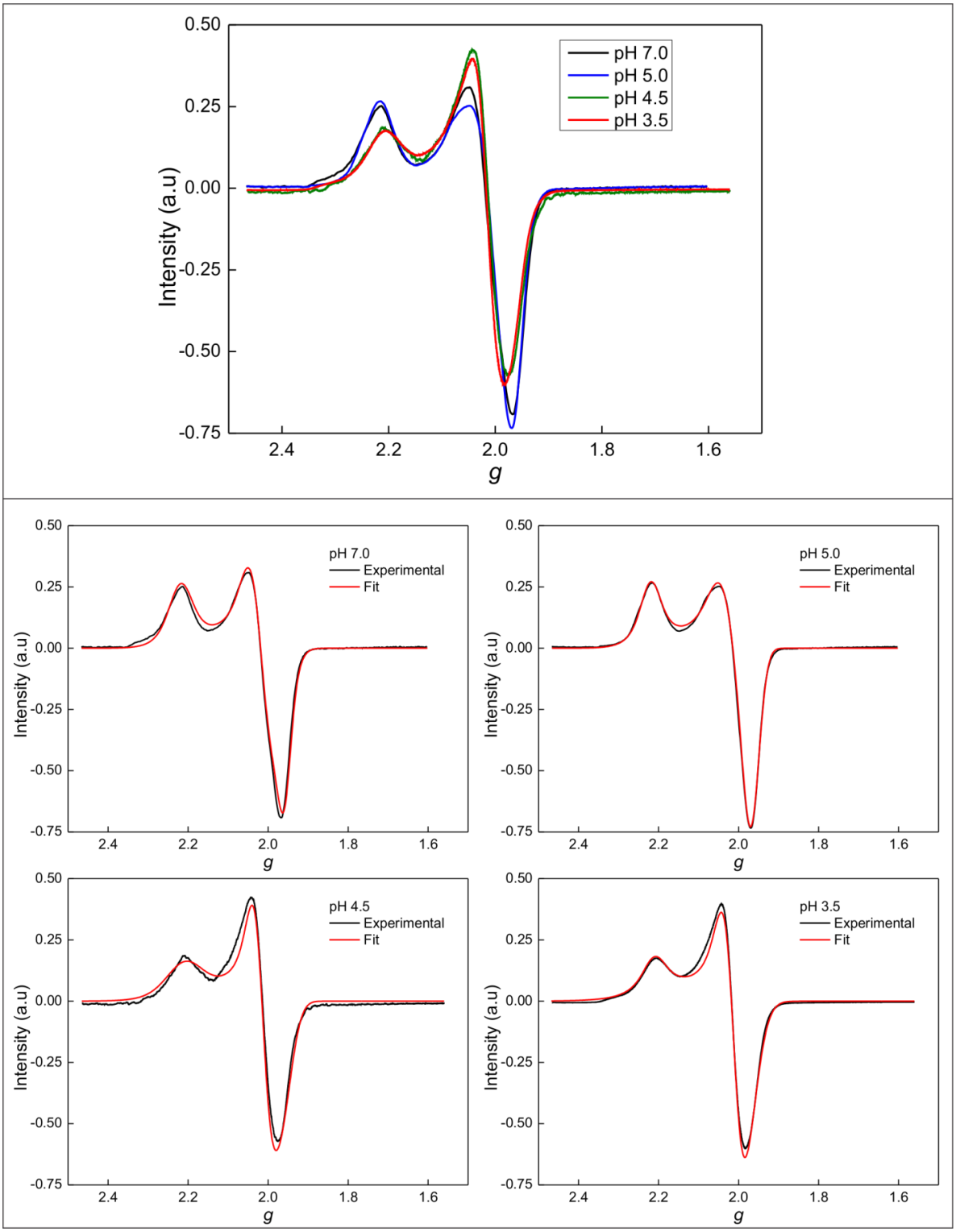

Figure S12. Top:EPR spectra of M160H acquired at different pH values. Visual inspection of the the spectra shows indeed a non-negligible change in the *g* values when lowering the pH. The hyperfine coupling *A*// could not be resolved at any of the studied pH values. The spectra can be grouped into two categories: neutral pH and low pH, suggesting a pH-dependent transition. Bottom: Fittings of the experimental curves from which the parameters presented in Table S2 were obtained.

Table S2. Fitted parameters obtained from the EPR spectra acquired at different pH values. The spectra were fitted by using the Easyspin tools based on MATLAB. The calculated $\Delta E_{\sigma_u^*/\pi_u}$ values suggest that at low pH there is an increase in the vertical energy gap corresponding with an increased population of the σ_μ* at lower pH, as concluded from the NMR experiment.

pH	g//[a][b]	$g\perp$[a]		A//	A⊥		ΔE[c]
7	2.219	2.02	1.96	60	40	40	4125.63
5	2.219	2.02	1.97	60	40	40	4125.63
4.5	2.212	2.01	1.96	60	40	40	4261.86
3.5	2.21	2.01	1.98	60	40	40	4302.45

[a]Initial g parameters were calculated from the magnetic field value. Given that the hyperfine coupling constants (A) are not resolved, we employed the parameters taken from the bibliography for this fitting[2], as a conservative approach. Once the *Hstrain* and *Gstrain* values were optimized, appropriate fitting of the g parameters was performed.

[b] The g// parameter decreases at low pH. This can be correlated to a possible protonation of the axial His with a concomitant weakening of the Cu-N_{His} bonds, that can be correlated with a loss of intensity of the N_{His}-Cu LMCT band. A similar explanation was put forward by the Solomon group to account for a similar pH-dependent transition in M123H Cu_A-Azurin.[7]

[c] The g// value also allows for estimation of the $\Delta E_{\sigma_u^*/\pi_u}$ [8] according to equation:

$$g_{||} = g_e + \frac{8\zeta_{3d}^{Cu}\alpha^2\beta^2}{\Delta}$$

It should be noted that the $\Delta E_{\sigma_u^*/\pi_u}$ value obtained from EPR experiments corresponds to a vertical transition from the σ_u^* GS to the excited π_u state, hence the larger values compared with those obtained from paramagnetic NMR determinations.

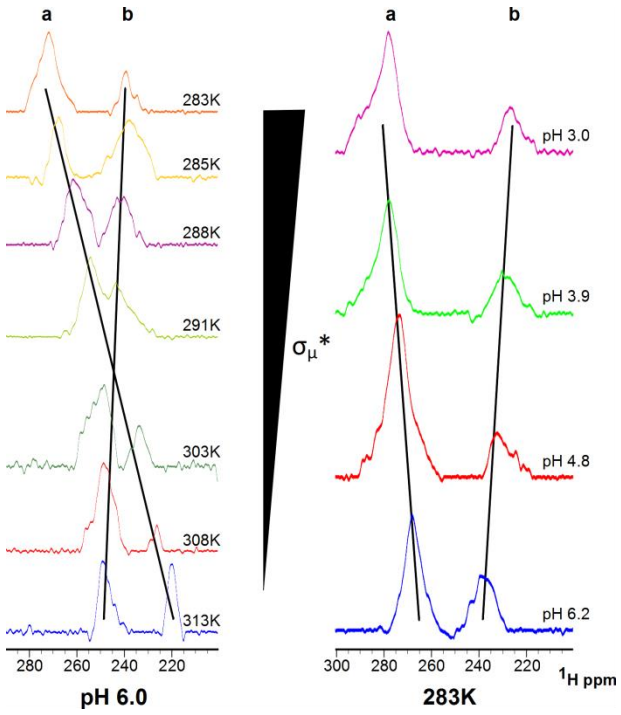

Figure S13. Temperature dependence (Left) and pH dependence (Right) of the *a* and *b* NMR signals (C153Hβ's1). The signals show the same behavior when lowering the pH as when the temperature decreases, indicating that the protein has a higher population of the σ_u* electronic level at low pH values.

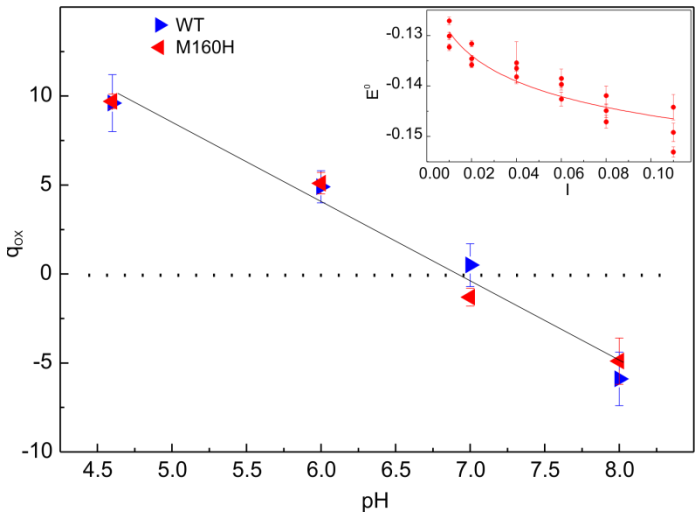

Figure S14. Determination of the isoelectric point (IP) of *Tt*-CuA (blue) and M160H (red) adsorbed on SAM coated electrodes. At each pH value, the charge of the protein was determined by assessing the dependence of Eº with the ionic strength (*I*) of the solution using the extended Debye-Hückel model.[9] This model allows for estimation of the charge of the protein at each pH value. For both *Tt*-CuA and M160H the pH at which the net charge is zero, corresponding to the IP, is *ca*. 7, representing an upshift of 1 pH unit from determinations of protein samples in solution.[10]

References

[1.] S. Stoll, A. Schweiger, *J. Magn. Reson.* **2006,** *178* 42-55.

[2.] S. Pfenninger, W. E. Antholine, M. E. Barr, J. S. Hyde, P. M. Kroneck, W. G. Zumft, *Biophys.J* **1995,** *69* 2761-2769.

[3.] M. Karpefors, C. E. Slutter, J. A. Fee, R. Aasa, B. K+ñllebring, S. Larsson, T. Vänngard, *Biophys. J.* **1996,** *71* 2823.

[4.] L. A. Abriata, D. Álvarez-Paggi, G. N. Ledesma, N. J. Blackburn, A. J. Vila, D. H. Murgida, *Proc. Natl. Acad. Sci. USA* **2012,** *109* 17348-17353.

[5.] E. Laviron, *J.Electroanal.Chem.Interfac.* **1979,** *101* 19-28.

[6.] M. J. Honeychurch, *Langmuir* **1999,** *15* 5158-5163.

[7.] M. L. Tsai, R. G. Hadt, N. M. Marshall, T. D. Wilson, Y. Lu, E. I. Solomon, *Proc. Natl. Acad. Sci. USA* **2013,** *110* 14658-14663.

[8.] S. I. Gorelsky, X. Xie, Y. Chen, A. James, E. I. Solomon, *J.Am.Chem.Soc.* **2006,** *128* 16452-16453.

[9.] J. Petrovic, R. A. Clark, H. Yue, D. H. Waldeck, E. F. Bowden, *Langmuir* **2005,** *21* 6308-6316.

[10.] C. E. Slutter, D. Sanders, P. Wittung, B. G. Malmström, R. Aasa, J. H. Richards, H. B. Gray, A. James, *Biochemistry* **1996,** *35* 3387-3395.